

MULTI-MATERIAL PRINTING TO SIMULTANEOUSLY ENHANCE INTERLAYER AND FLEXURAL PERFORMANCE IN 3D CONCRETE PRINTING

FEI TENG^{*}, JUNHONG YE[†], JIE YU^{*}, AND YIWEI WENG^{*}

^{*} Department of Building and Real Estate, The Hong Kong Polytechnic University, Hong Kong, China

[†] Institute of Smart City and Intelligent Transportation, Southwest Jiaotong University, Chengdu, China

Corresponding Author: yiwei.weng@polyu.edu.hk

Key words: 3D Concrete Printing, Multi-material Printing, Strain-hardening Cementitious Composites, Interlayer Performance, Flexural Performance

Abstract: The layer-atop-layer construction process in 3D concrete printing (3DCP) has incurred two limitations: (1) the weak interlayer bond strength and (2) the difficulty of integrating steel reinforcement. Strain-hardening cementitious composites (SHCC) with high tensile properties have the potential to achieve self-reinforced structures in 3DCP. This study proposes a multi-material printing strategy by combining ductile (SHCC) and brittle (printable mortar) cementitious materials to address these two limitations simultaneously. SHCC are used as the bonding agents introduced at the interfaces of printed mortar. A dual-nozzle system is designed to achieve synchronized SHCC deposition and mortar printing. The splitting tensile test was adopted to evaluate the interlayer bond strength and four-point bending test was performed to study the flexural performance. The results show that the SHCC bonding agents can enhance the interlayer bond strength by 80% and reduce the interfacial porosity by 35%. In the SHCC-concrete beams, the flexural strength, deflection, and energy absorption capacity increase by 26%, 182%, and 800%, respectively, compared to the reference group without SHCC. The findings reveal that the proposed multi-material printing strategy has great potential to address the weak interlayer bond strength and reinforcement integration problems in 3DCP.

1 INTRODUCTION

3D concrete printing (3DCP) has developed rapidly in recent years for the benefits of enhanced sustainability and productivity. However, the traditional 3DCP process typically uses a single material, i.e., cement mortar, for printing. The inherent brittleness of cementitious material requires sufficient reinforcement to bear the tensile load and enhance ductility. However, the layer-atop-layer construction process in 3DCP is difficult to introduce traditional steel reinforcement [1]. Additionally, this unique layer-stacking manner incurs weak interlayers between printed mortar layers. These two limitations in traditional 3DCP compromise the mechanical properties

of printed components, impeding the wide structural application of 3DCP.

Existing studies have explored several methods to address the above-mentioned two limitations. For the weak interlayer problem, various methods including optimizing the printing parameters [2], tailoring surface moisture content [3], and controlling the time gap between layers [4], have been proposed. The addition of bonding agents between layers is also an effective method. Weng et al. [5] have used cement-based bonding agents with a dual-nozzle system. The interlayer bond strength can be improved by 267% compared to the reference group. However, a detailed investigation of material aspects is lacking. In

particular, the effect of bonding material on the interlayer microstructure and failure mechanism are yet unexplored.

To address the steel reinforcement integration problem, traditional steel rebars can be manually placed in the printed structures [6]. Nevertheless, the additional manual work conflicts with the automated process of 3DCP. The automatic process such as the continuous steel cable [7] and carbon yarn [8] has limited mechanical improvement and requires complex external facilities. The in-process rebar printing using laser welding has low productivity and is energy-consuming [9].

Strain-hardening cementitious materials (SHCC), with a high tensile strength and tensile strain capacity, have the potential to achieve self-reinforced structures [10]. However, directly using SHCC as the printable material is easy to cause fibre agglomeration during the extrusion process [11]. To address this problem, high-flowable SHCC can be used as bonding agents, which are driven by gravitational force, eliminating the need for pumping and extrusion processes.

Based on the above analysis, this study proposes a multi-material printing strategy to simultaneously improve the interlayer and flexural performance in 3DCP. Specifically, this strategy combines ductile (SHCC) and brittle (printable mortar) cementitious material to form a composite structure. SHCC are used as the bonding agents introduced at the interfaces of printed mortar. A novel dual-nozzle system is designed to achieve synchronized mortar printing and SHCC deposition. Two research questions are further explored: (1) how the rheological properties of SHCC affect the interlayer performance, and (2) how the configuration of SHCC layers affects the flexural performance. Three SHCC mixtures with different viscosity modifying agent (VMA) dosages were designed. Splitting tensile tests were adopted to evaluate the interlayer bond strength, and four-point bending test was performed on the multi-layer composite SHCC-concrete beams to investigate the flexural performance.

2 METHODOLOGIES

2.1 Materials and nozzle design

Two types of materials are used in this study, including the SHCC bonding agents and the printable mortar. Table 1 presents the mixture proportions of SHCC bonding agents. Ordinary Portland cement (OPC), class F fly ash (FA), silica fume (SF), and quartz sand were blended as the raw materials. A superplasticizer (SP) was used to tailor the workability of SHCC. Polyethylene (PE) fibres with a volume fraction of 1% were added to improve the tensile properties. Three viscosity modifying agent (VMA) dosages, by the mass fraction of cement at 0%, 0.15%, and 0.25%, were adopted to achieve different rheological properties. FA, SF, HRWR, and VMA were supplied by Shanghai Siqi Building Materials Co., Ltd.

Table 2 shows the mixture proportions of printable mortar, which consists of OPC, a commercial premixed plaster (BP138, Optimix Hong Kong), and SF. Polypropylene (PP) fibres with a volume fraction of 0.5% were used to mitigate drying shrinkage during the curing period. The mechanical properties of PE and PP fibres are presented in Table 3.

Table 1: Mixture proportion of SHCC bonding agents (Unit: kg/m³)

Mixture	OPC	FA	SF	Sand	PE fibre	Water	SP	VMA
VMA-0								0
VMA-0.15	609	561	79	381	10	390	6	0.91
VMA-0.25								1.52

Table 2: Mixture proportion of printable mortar (Unit: kg/m³)

OPC	BP138	SF	Water	PP fibre
798	709	76	433	4.1

Table 3: Mechanical properties of PE and PP fibres

Fibre type	Length (mm)	Diameter (μm)	Aspect ratio	Tensile Strength (MPa)	Elastic Modulus (GPa)
PE	12	24	500	2900	116
PP	6	12	500	910	9

The SHCC bonding agents and printable mortar were mixed separately using two mixers. Firstly, dry powders were blended and mixed for 1 minute at a low speed (140 rpm for printable mortar; 800 rpm for SHCC). Then, water was added and mixed at the same speed for another 1 minute. Afterwards, a high mixing speed (420 rpm for printable mortar; 1130 rpm for SHCC) was adopted for 3 minutes. Finally, fibres (PP fibres for printable mortar; PE fibres for SHCC) were added, and all the materials were mixed at high speed until the fibres were well dispersed. The rheological properties, including the dynamic yield stress and plastic viscosity, as well as the tensile properties of the three SHCC bonding agents were tested. Figure 1 shows the setup of the printing scheme. A robot printer (ABB IRB2600) was used for printing with a constant travelling speed of 30 mm/s.

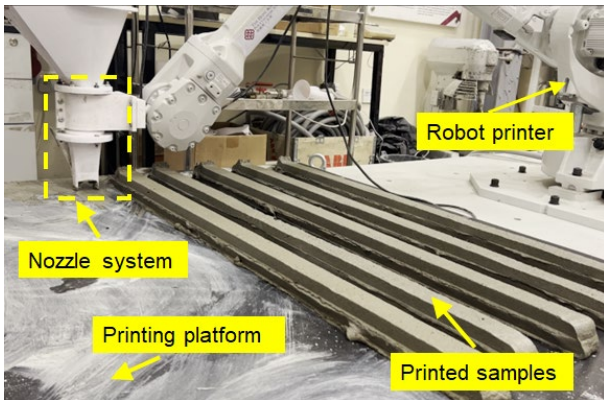
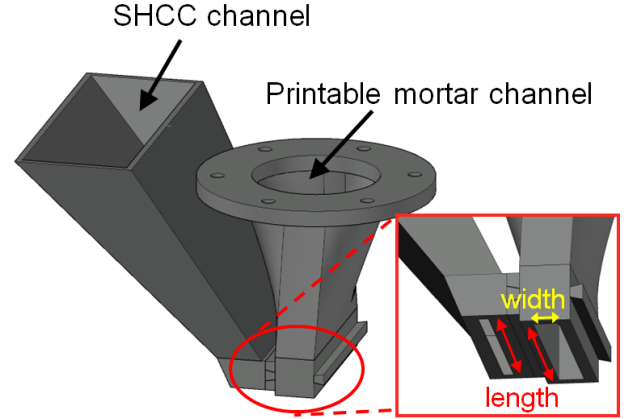
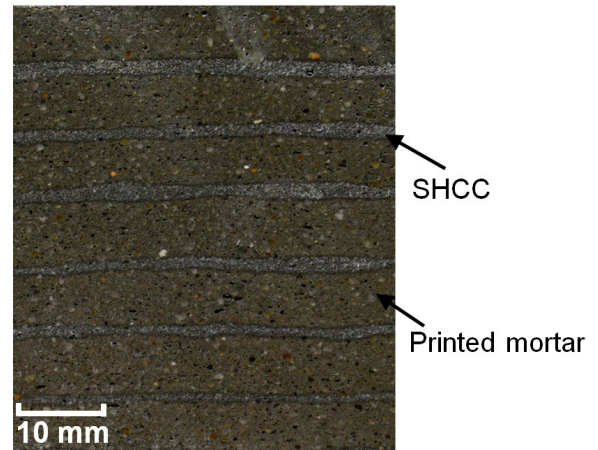

Figure 1: Setup of the printing system

Figure 2 shows the schematic of the newly designed dual-nozzle system [6]. The main channel was used for mortar printing and the side channel was used for SHCC deposition, respectively. The two channels have the same outlet length to ensure that SHCC can be deposited on the entire surface of the printed mortar. Figure 3 shows the picture of a cross-section cut from a multi-layer structure printed

with the designed dual-nozzle. As can be seen from Figure 3, the SHCC bonding agents can be introduced at the interfaces of the printed mortar layers.


Figure 2: The schematic of the dual-nozzle system

Figure 3: Cross-section of samples printed with the dual-nozzle system

2.2 Mechanical test

In this study, the splitting tensile test and four-point bending test were adopted to study the interlayer and flexural performance, respectively. Figure 4 shows the schematic of the test. For the splitting tensile test (Figure 4a), the specimen had two layers of printed mortar with the SHCC bonding agent at the interface. The three SHCC bonding agents shown in Table 1 were used for the printing. A reference group without SHCC was also printed. The layer height of printed mortar was 20 mm and the length of the sample was 50 mm. Two steel strips were fixed at the top and bottom side of

the specimen. The loading rate was 0.1 mm/min. Five replicates were tested for each group. The interlayer bond strength (f_t) is calculated by:

$$f_t = \frac{2P_u}{\pi A} \quad (1)$$

Where P_u and A represent the maximum load and the interfacial area, respectively. μ CT technique (XT H 225 ST, Nikon) was also employed on the same specimens to investigate interfacial porosity. The scanning voltage, current, and pixel size were 108 kV, 100 μ A, and 20 μ m, respectively.

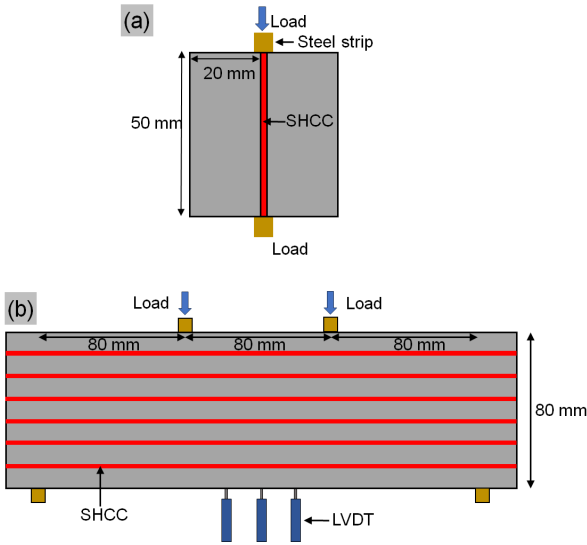


Figure 4: Schematic of the mechanical test: (a) Splitting tensile test; (b) Four-point bending test

For the four point-bending tests (Figure 4b), multi-layer beam members were printed with the dimensions of 80 mm \times 80 mm \times 320 mm ($W \times H \times L$). The SHCC mixture that achieves the highest interlayer performance was used in this test. To investigate how the configurations (location and volume fraction) of SHCC can affect flexural performance, four different SHCC configurations were designed, as shown in Figure 5. SCB-8-7 indicates the SHCC-concrete beam (SCB) has 8 layers of printed mortar and 7 layers of deposited SHCC bonding agents. Three linear variable displacement transducers (LVDTs) with a sampling frequency of 1 Hz were installed at the middle bottom of the specimen to measure the mid-span deflection. The load was applied in the direction perpendicular to the printing direction.

Three replicates were tested for each group with a loading rate of 0.2 mm/min. The flexural stress is calculated as:

$$f = \frac{PL}{bd^2} \quad (2)$$

Where P is the applied load. L is the span of the beam. b and d are the width and height of the beam, respectively.

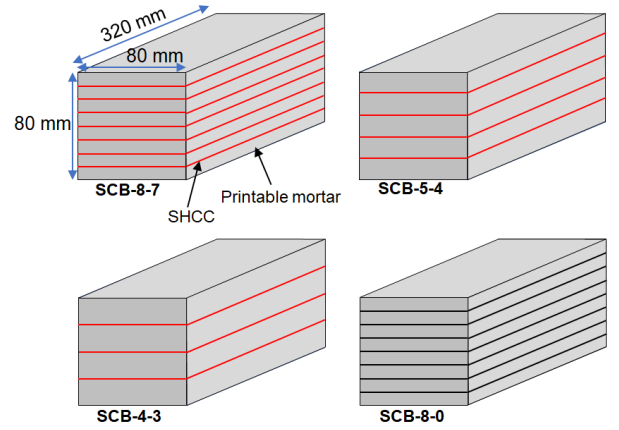


Figure 5: Specimen design of the composite SHCC-concrete beams

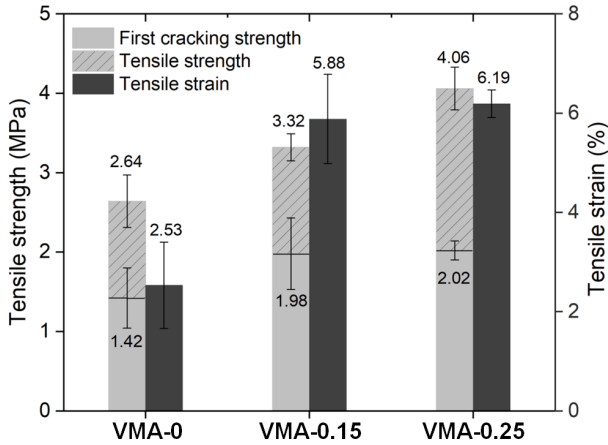
3 RESULTS

3.1 Fresh and hardened properties of SHCC

Table 4 presents the rheological properties of the three types of SHCC bonding agents. Figure 6 shows the summarized tensile properties. With the increase in VMA dosage, both the rheological properties and the tensile properties are improved. Compared to the reference group without VMA, the first cracking strength, tensile strength, and tensile strain capacity of the mixture VMA-0.25 are improved by 42%, 54%, and 145%, respectively. The enhanced tensile properties are attributed to the increase of plastic viscosity from 1.26 Pa·s to 2.62 Pa·s. Higher plastic viscosity is beneficial for fibre dispersion in the cement matrix. Another reason is that the increased dynamic yield stress and plastic viscosity in VMA-0.25 can decrease the bleeding.

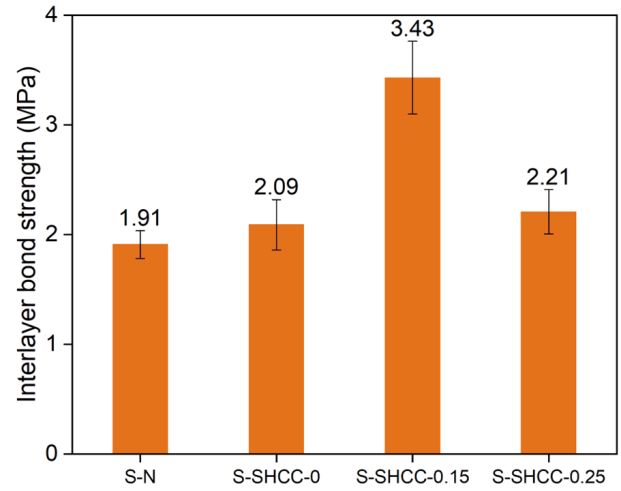
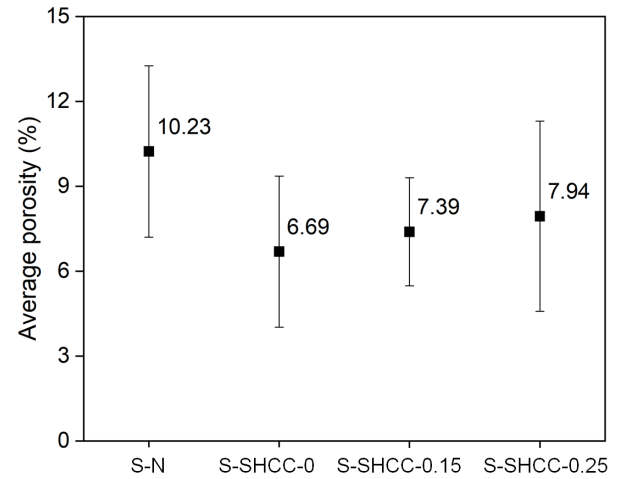
Table 4: Rheological properties of SHCC

SHCC ID	Dynamic yield stress (Pa)		Plastic viscosity (Pa·s)	
	Mean value	Standard deviation	Mean value	Standard deviation
VMA-0	98.37	4.85	1.26	0.18
VMA-0.15	123.73	10.12	1.64	0.07
VMA-0.25	138.88	6.18	2.62	0.11


Figure 6: Summarized tensile properties of SHCC

3.2 Interlayer bond strength

Figure 7 shows the results of the splitting tensile test, and Figure 8 shows the results of interfacial porosity obtained from the μ CT test. Compared to the reference group without SHCC bonding agents (S-N), the addition of SHCC bonding agents can effectively enhance the interlayer bond strength, meanwhile reducing the interfacial porosity. When the SHCC with 0.15% VMA is used as the bonding agent, the specimen achieves the highest interlayer bond strength of 3.43 MPa, which is 80% higher than that of S-N. The specimen S-SHCC-0 has the lowest interfacial porosity of 6.69%, which is reduced by 35% compared to that of the reference group.


Figure 7: Results of splitting tensile test

Figure 8: Interfacial porosity with different bonding agents

The rheological properties of SHCC bonding agents can highly affect the interlayer bond strength. The interlayer bond strength of S-SHCC-0 and S-SHCC-0.25 are lower than that of S-SHCC-0.15. Figure 9 shows the failure modes of specimens after the splitting tensile test. With the addition of SHCC bonding agents, two new interfaces are formed at the original interfacial region. As shown in Figure 9 (b), the specimen fractures at the matrix of SHCC (the area between the two yellow lines), other than at the new interfaces, indicating the first cracking strength of SHCC determines the interlayer bond strength. Therefore, S-SHCC-0 has a lower interlayer bond strength due to the decreased first cracking strength, compared to that of S-SHCC-0.15 (Figure 6). The lower

interlayer bond strength of S-SHCC-0.25 is attributed to the compromised interfacial microstructure. From the results of the μ CT test, S-SHCC-0 has the highest proportion of macro pores (diameter larger than 100 μm) at 55.1%, which typically exhibit irregular geometries. When the splitting tensile load is applied at the interface, S-SHCC-0.25 has a more severe stress concentration occurring at these macro pores, causing the reduction of interlayer bond strength.

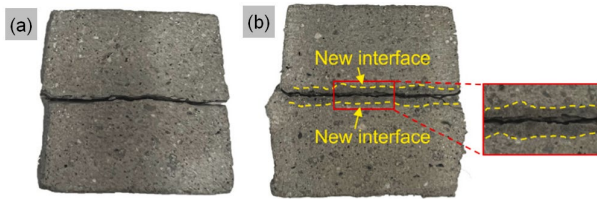


Figure 9: Failure modes after splitting tensile tests: (a) without SHCC; (b) with SHCC

3.3 Flexural performance

Figure 10 (a) plots the flexural stress versus mid-pan deflection curves of the composite SHCC-concrete beams in the four-point bending test. Three types of flexural behaviours can be observed: (1) flexural hardening (SCB-8-7), in which the flexural stress reaches a second peak higher than the initial cracking stress; (2) flexural pseudo-hardening (SCB-5-4), in which the flexural stress at the second peak is lower than the initial cracking stress and (3) quasi-brittle failure (SCB-4-3 and SCB-8-0), in which the specimens exhibit a sudden failure after the initial cracking. The above results indicate that with an appropriate SHCC configuration, the failure mode of the specimens under flexural loading can achieve the transition from quasi-brittle failure to ductile failure, thereby improving the ductility of the printed beam member.

Figure 10 (b) shows the summarized flexural strength and the corresponding deflection. An increased flexural strength can be achieved with the addition of the SHCC bonding agents due to the enhanced interlayer bond strength. The flexural strength of SCB-8-7, SCB-5-4, and SCB-4-3 is improved by 26%, 11%, and 10%, respectively, compared to that of SCB-8-0 (5.21 MPa). The peak deflection of SCB-8-7 is 0.96

mm, which is 182% higher than that of SCB-8-0 (0.34 mm). Figure 10 (c) shows the energy absorption capacity, which is defined as the area underneath the flexural stress-deflection curve when the stress drops to 85% of the flexural stress at the second peak. SCB-8-7 with the flexural hardening behaviour has the highest energy absorption capacity, indicating superior flexural ductility, followed by the flexural pseudo-hardening of SCB-5-4. The enhancement of energy absorption capacity is due to the fibre-bridging effect of SHCC bonding agents, which can inhibit the propagation of the critical crack.

4 CONCLUSIONS

This study proposes a multi-material printing strategy in 3D concrete printing (3DCP) to simultaneously address the weak interlayer and reinforcement integration problems. Ductile strain-hardening cementitious composites (SHCC) and brittle printable mortar are combined to form a novel composite structure. SHCC are used as bonding agents at the interfaces of printed mortar. A novel dual-nozzle system is designed to achieve synchronized SHCC deposition and mortar printing. Splitting tensile test and four-point bending test are adopted to evaluate the interlayer and flexural performance, respectively. The main conclusions are as follows:

- (1) With the addition of SHCC bonding agents, the interlayer bond strength can be improved by 80% and the interfacial porosity can be reduced by 35%.
- (2) For the flexural performance, the flexural strength, deflection, and energy absorption capacity of SCB-8-7 are 26%, 182%, and 800% higher than those of the reference specimen without SHCC.

5 ACKNOWLEDGEMENTS

The author would like to gratefully acknowledge the Project No.52308284 supported by National Natural Science Foundation of China. The work described in this paper was also supported by a grant from

the Germany/Hong Kong Joint Research Scheme sponsored by the Research Grants Council of Hong Kong and the German Academic Exchange Service (Reference No. G-PolyU503/23), and Guangdong Basic and Applied Basic Research Foundation (No. 2024A1515011870).

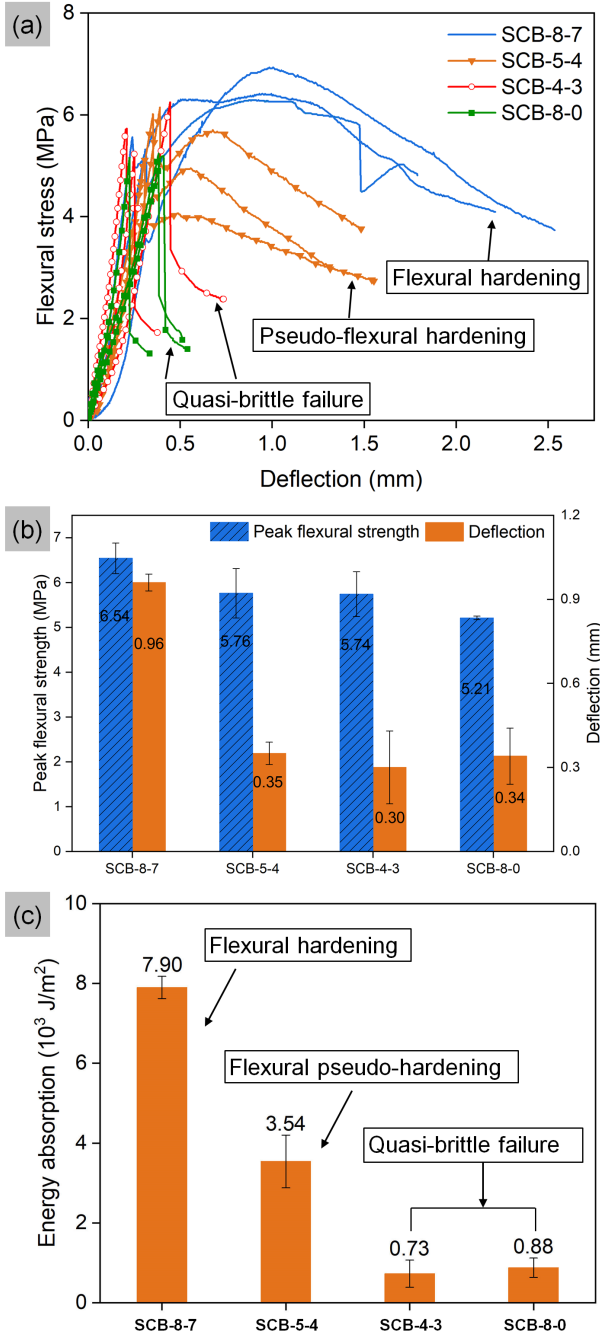


Figure 10: Results of four-point bending tests: (a) Flexural stress-deflection curves; (b) Summarized flexural strength and corresponding deflection; (c) Energy absorption capacity

REFERENCES

- [1] Du, S., Teng, F., Zhang, D., Li, M., Li, H. and Weng, Y., 2024. A BIM-enabled robot control system for automated integration between rebar reinforcement and 3D concrete printing, *Virtual Phys. Prototyp.* **19** 1–20.
- [2] Weng, Y., Li, M., Zhang, D., Tan, M.J. and Qian, S., 2021. Investigation of interlayer adhesion of 3D printable cementitious material from the aspect of printing process, *Cem. Concr. Res.* **143** 106386.
- [3] Sanjayan, J.G., Nematollahi, B., Xia, M. and Marchment, T., 2018. Effect of surface moisture on inter-layer strength of 3D printed concrete, *Constr. Build. Mater.* **172** 468–475.
- [4] Tay, Y.W.D., Ting, G.H.A., Qian, Y., Panda, B., He, L. and Tan, M.J., 2019. Time gap effect on bond strength of 3D-printed concrete, *Virtual Phys. Prototyp.* **14** 104–113.
- [5] Weng, Y., Li, M., Wong, T.N. and Tan, M.J., 2019. Synchronized concrete and bonding agent deposition system for interlayer bond strength enhancement in 3D concrete printing, *Autom. Constr.* **123** 103546.
- [6] Zhu, B., Nematollahi, B., Pan, J., Zhang, Y., Zhou, Z. and Zhang, Y., 2021. 3D concrete printing of permanent formwork for concrete column construction, *Cem. Concr. Compos.* **121** 104039.
- [7] Ma, G., Li, Z., Wang, L. and Bai, G., 2019. Micro-cable reinforced geopolymer composite for extrusion-based 3D printing, *Mater. Lett.* **235** 144–147.
- [8] Neef, T., Müller, S. and Mechtcherine, V., 2024. Integrating continuous mineral-impregnated carbon fibers into digital fabrication with concrete, *Mater. Des.* **239** 112794.

- [9] Mechtcherine, V., Grafe, J., Nerella, V.N., Spaniol, E., Hertel, M. and Füssel, U., 2018. 3D-printed steel reinforcement for digital concrete construction – Manufacture, mechanical properties and bond behaviour, *Constr. Build. Mater.* **179** 125–137.
- [10] Ye, J., Teng, F., Yu, J., Yu, S., Du, H., Zhang, D., Ruan, S. and Weng, Y., 2023. Development of 3D printable engineered cementitious composites with incineration bottom ash (IBA) for sustainable and digital construction, *J. Clean. Prod.* **422** 138639.
- [11] Xu, N. and Qian, Y., 2023. Effects of fiber volume fraction, fiber length, water-binder ratio, and nanoclay addition on the 3D printability of strain-hardening cementitious composites (SHCC), *Cem. Concr. Compos.* **139** 105066.